Check for updates

Hybrid quantum systems with circuit quantum electrodynamics

A. A. Clerk[1], K. W. Lehnert [2,3,4], P. Bertet[5], J. R. Petta [6] and Y. Nakamura [7,8] ✉

The rise of quantum information science has provided new perspectives on quantum mechanics, as well as a common language for quantum engineering. The focus on platforms for the manipulation and processing of quantum information bridges between different research areas in physics as well as other disciplines. Such a crossover between borders is well embodied by the development of hybrid quantum systems, where heterogeneous physical systems are combined to leverage their individual strengths for the implementation of novel functionalities. In the microwave domain, the hybridization of various quantum degrees of freedom has been tremendously helped by superconducting quantum circuits, owing to their large zero-point field fluctuations, small dissipation, strong nonlinearity and design flexibility. These efforts take place by expanding the framework of circuit quantum electrodynamics. Here, we review recent research on the creation of hybrid quantum systems based on circuit quantum electrodynamics, encompassing mechanical oscillators, quantum acoustodynamics with surface acoustic waves, quantum magnonics and coupling between superconducting circuits and ensembles or single spins.

In undergraduate and graduate courses on solid-state physics, we learn a lot about particles and quasiparticles, such as electrons, holes, spins, plasmons, phonons, magnons and many more, as quanta of excitations in condensed-matter systems. However, not many have considered controlling and measuring the quantum states of those degrees of freedom at the level of a single quantum, until the rise of quantum information science taught us the potential of such technologies.

The demonstration of a superconducting qubit was an early example of the coherent control of a quantum in a collective mode in a circuit[1,2]. Soon after, inspired by results obtained by cavity quantum electrodynamics (cavity QED) coupling atoms and photons[3], the concept of circuit quantum electrodynamics (circuit QED) was introduced[4–6]. In circuit QED, superconducting qubits acting as artificial atoms strongly interact with microwave photons in resonators. Since then, a generic and successful strategy has been to extend the circuit-QED approach towards other quantum degrees of freedom, exploring new physics emerging from the advanced control and measurement techniques in hybridized setups and expanding the array of systems that may be exploited for quantum technologies (Fig. 1). A number of breakthrough demonstrations of hybrid quantum systems based on circuit-QED techniques have been reported, and more are expected to follow.

Interdisciplinary by nature, hybrid quantum systems catalyse novel ideas at the frontier of research. They can be utilized for fundamental research in quantum mechanics, mesoscopic physics and condensed-matter physics, providing platforms and tools to investigate deeper into the previously unexplored quantum regimes. These systems are also expected to be useful for a variety of applications in quantum technologies, for example, as quantum-limited sensors and transducers, or as quantum buses and memories.

This article reviews notable achievements and the main challenges for the development of hybrid quantum systems based on circuit QED, with an emphasis on their unique properties. Here, we focus exclusively on systems operating in the microwave domain, leaving the vast parallel activities in the optical domain to be covered elsewhere. Earlier and recent reviews on related topics can be found in refs. [7–17].

In the following, we summarize the theoretical background relevant for hybrid quantum systems in circuit QED. We then cover the latest progress in representative realizations of hybrid quantum systems.

The basics of circuit-QED hybrid systems

In terms of quantum-state engineering and manipulation, different quantum systems typically have disparate advantages and disadvantages. Some have strong nonlinearities, enabling the complex processing of quantum states (for example, superconducting circuits incorporating Josephson elements), whereas others have extremely long coherence times that are ideal for the storage of quantum states (for example, ensembles of atomic or solid-state spins). The broad goal of hybrid quantum systems is to develop integrated platforms that simultaneously exploit the complementary advantages of two or more different physical systems. Both the utility and difficulty of developing such hybrid systems are obvious. In fact, couplings between excitations of very different physical systems are often extremely weak, and the natural excitation frequencies of the degrees of freedom of interest are in many cases quite different — another hurdle towards their direct coupling.

The circuit-QED toolkit provides a uniquely powerful route for constructing a variety of hybrid quantum systems. The goal is to coherently couple circuit-QED degrees of freedom (microwave cavity photons, the state of a superconducting qubit) to a completely different physical degree of freedom (for example, mechanical phonons, optical photons, spin wave excitations of a ferromagnet).

The most basic kind of hybrid interaction is the so-called beamsplitter linear interaction, the details of which are discussed in Box 1. The success of conventional circuit QED stems from the
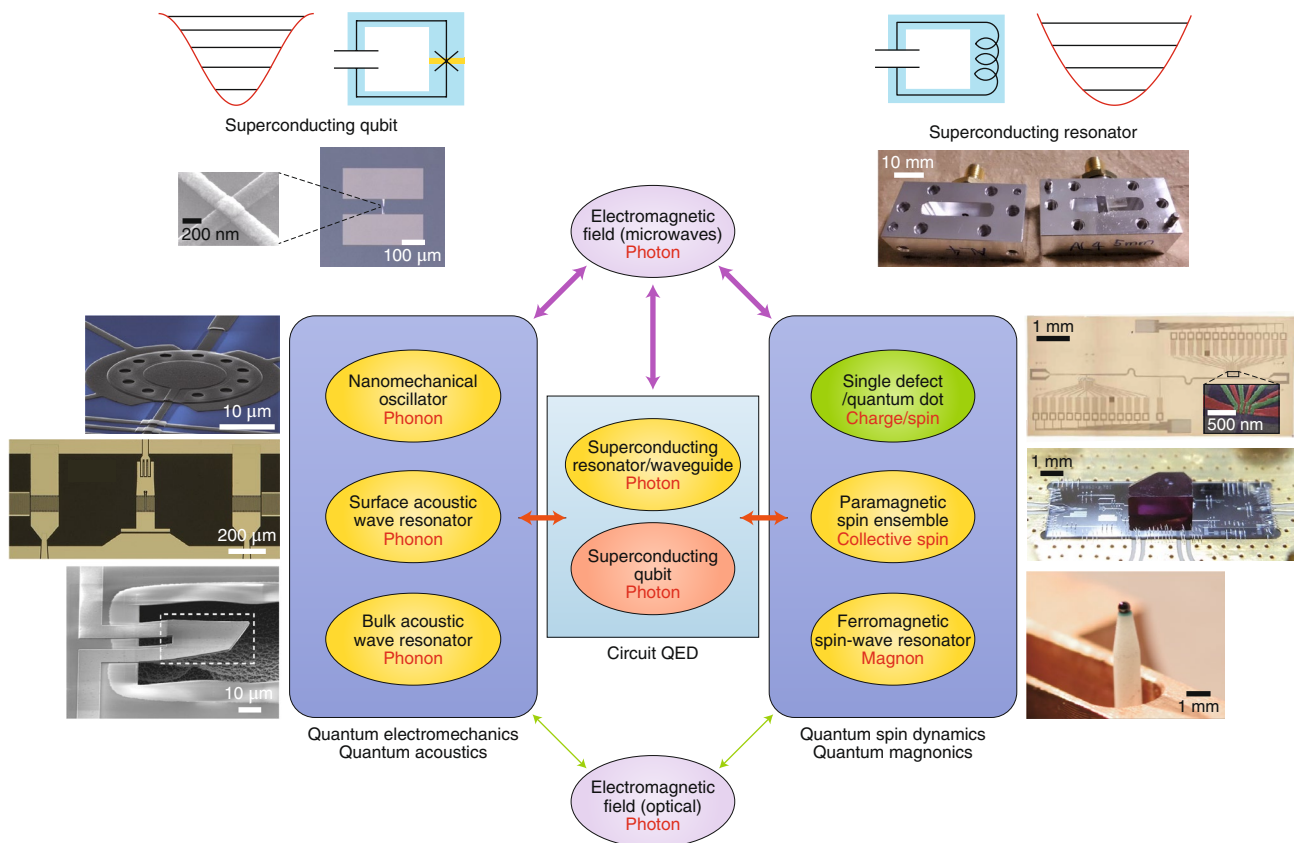
Fig. 1 | Hybrid quantum systems with circuit QED. The excitations in the core elements — superconducting qubits, resonators and waveguides — are often referred to as '(microwave) photons' for simplicity, but can more precisely be understood as surface plasmon polaritons, that is, quanta of the composite modes of the surface charge-density waves in a superconducting circuit and the near-field electromagnetic waves. Owing to the nonlinearity of a Josephson junction (indicated with a cross in the top-left schematic), the qubit acquires strong anharmonicity. Collective excitation modes other than the superconducting qubit and the single charge/spin excitations are represented by yellow items. The corresponding quanta are indicated in red. All these degrees of freedom couple coherently with microwaves (purple arrows) and with superconducting circuits (red arrows). Coupling schemes with largely detuned photons in the optical domain compatible with the cryogenic environment for circuit QED are currently under development (green arrows)[15–17]. Arrow thickness indicates the relative strength of the coupling. The pictures show, clockwise from the top left, a superconducting transmon qubit (the left panel is a close-up of a Josephson junction), a three-dimensional superconducting resonator, gate-defined quantum dots coupled to a superconducting coplanar-waveguide resonator, a diamond crystal containing an ensemble of spins placed on a superconducting resonator chip[77], a ferromagnetic sphere of YIG embedded in a copper-made microwave cavity[55], a film bulk acoustic resonator made of AlN sandwiched with Al electrodes[26], a surface acoustic resonator fabricated on a quartz substrate[43] and a drumhead-type Al membrane nanoelectromechanical oscillator[106]. Figure adapted with permission from: bottom-left image, ref. [26], Springer Nature Ltd; centre-left image, ref. [43], Springer Nature Ltd.

extremely strong couplings that can be achieved between a qubit and a superconducting cavity. These arise from the large zero-point field fluctuations in these cavities, which result from small mode volumes. Crucially, these large cavity zero-point fluctuations also enable potentially sizeable coupling to other physical systems. There are two basic methods for generating hybrid beamsplitter couplings in circuit QED. One option is to couple a system capacitively to the electric field or voltage associated with the cavity mode. For the simple case where the microwave cavity mode can be modelled as an inductor–capacitor (LC) resonator, the coupling strength g will be proportional to the magnitude of the cavity mode's zero-point voltage fluctuations $V_{zpt} = \omega_0 \sqrt{\hbar Z/2}$, where $\omega_0 = 1/\sqrt{LC}$ is the resonator frequency, $Z = \sqrt{L/C}$ its characteristic impedance, L is the inductance, C is the capacitance and $\hbar$ is Planck's constant/2π. Achieving large couplings in this case requires high-impedance microwave resonators. An alternative route is to couple a system inductively to the magnetic field or current associated with the cavity mode. Again, taking the cavity to be a simple LC circuit, g will be proportional to the size of the cavity zero-point current fluctua-

tions $I_{zpt} = \omega_0 \sqrt{\hbar/2Z}$. Here, large couplings are obtained when resonators have small impedances Z. The parameter that serves as a dimensionless measure of hybrid coupling strength is the cooperativity $\mathcal{C}$, as discussed in Box 2.

For hybrid quantum systems, the advantages of circuit-QED platforms are not limited to the size of the couplings. The strong nonlinearity provided by superconducting circuits is also a key resource. As discussed in a review by Blais et al.[18], a Josephson junction acts as an effective nonlinear inductance, and thus can provide strong nonlinearity for microwave photons at the quantum level. Engineering a hybrid coupling like the beamsplitter Hamiltonian $\hat{H}_{BS}$ in Eq. (1) allows a second system to exploit this nonlinearity, even if the coupling itself is purely linear.

Hybrid couplings that are intrinsically nonlinear — and not simply bilinear in bosonic raising and lowering operators — can also be engineered through the Josephson-junction-induced nonlinearity. A simple example is a so-called dispersive coupling. Starting with the beamsplitter interaction in Eq. (1), we add two simple ingredients: a frequency detuning Δ between the two systems, and a Kerr-type

Box 1 | Coupling hybrid systems in circuit QED

The simplest kind of hybrid-systems interaction is one which coherently and resonantly transfers excitations between two systems A and B:

$$\hat{H}_{\mathrm{BS}} = \hbar g \left(\hat{a}^\dagger \hat{b} + \hat{b}^\dagger \hat{a} \right) \qquad (1)$$

Here $\hat{a}^\dagger$ $(\hat{b}^\dagger)$ creates an excitation in system A (B), and $\hat{a}$ $(\hat{b})$ removes an excitation from system A (B). The unitary dynamics generated by $\hat{H}_{\mathrm{BS}}$ causes single excitation states to oscillate (Rabi flop) between the A and B systems at a frequency g/π. For circuit-QED hybrid platforms, the A system is typically a resonant mode of a superconducting microwave cavity, and thus $\hat{a}$ is just a canonical bosonic annihilation operator. In many cases, $\hat{b}$ is also a canonical annihilation operator, making $\hat{H}_{\mathrm{BS}}$ a standard beamsplitter interaction. Even in this linear regime, circuit-QED architectures offer many advantages: they allow one to realize this paradigmatic hybrid coupling with large couplings, low dissipation and a well-controlled environment.
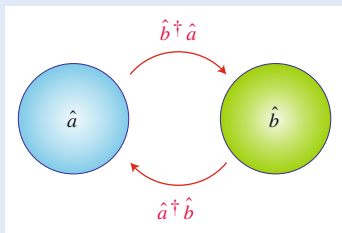
Intrinsically nonlinear couplings can also be engineered in circuit QED. One example is parametric couplings, as discussed in the main text. Letting A represent a microwave cavity mode, these generically have the form

$$\hat{H}_{\mathrm{P}} = g_{\mathrm{P}} \left(\hat{a} + \hat{a}^\dagger \right)^2 \left(\hat{b} + \hat{b}^\dagger \right)$$

Alternatively, nonlinear dispersive couplings can be generated by starting with a linear beamsplitter coupling with a large detuning and a nonlinearity in one of the two systems. The Hamiltonian in this case takes the form:

$$\hat{H}_{\mathrm{D}} = \chi \hat{a}^\dagger \hat{a} \hat{b}^\dagger \hat{b} \qquad (2)$$

For weak nonlinearities U, one has $\chi \propto U(g/\Delta)^2$, whereas for strong nonlinearity, $\chi \propto g^2/\Delta$, where Δ is the frequency detuning between the two systems.

Schematic of a basic 'beamsplitter' style linear interaction that coherently transfers excitations between two systems.

nonlinearity in one of them — typically the superconducting Josephson circuit. For a large frequency detuning, the beamsplitter interaction is unable to act to first order, as excitations cannot be transferred in a manner that conserves energy. To second order, however, processes involving virtual excitation transfer lead to an effective interaction between the systems that conserves their individual excitation number. This makes the excitation energy of one system depend on the other, and vice versa. Such dispersive interactions are extremely useful for quantum measurement and state manipulation. In the hybrid context, they are an indispensable resource for systems where it is infeasible to bring both systems into resonance.

Another widespread approach for the realization of nonlinear couplings is the engineering of parametric couplings, where a system is coupled to a microwave LC resonator by effectively modulating either its capacitance or its inductance. For example, in electromechanical systems, the capacitance is modulated by the position $\hat{x} \propto \hat{b} + \hat{b}^\dagger$ of a mechanical resonator, where $\hat{b}$ $(\hat{b}^\dagger)$ is the phonon annihilation (creation) operator. The complementary coupling, where it is the cavity inductance that is modulated by a second system, can be achieved by using a pair of Josephson junctions in a superconducting quantum interference device (SQUID) configuration to provide the effective cavity inductance. Such a setup effectively acts like a flux-dependent inductance. By modulating this external flux, one again gets a parametric coupling. Nonlinear parametric couplings are extremely useful, as they can be enhanced and manipulated by applying simple classical coherent drives to the microwave cavity. As discussed below, this allows one to realize tunable beamsplitter interactions even between systems with very different natural frequencies.

Finally, yet another powerful advantage of circuit-QED platforms for hybrid quantum systems is the ability to generate non-classical microwave states that can be exploited for enhanced quantum transduction. Recent theoretical work has demonstrated that microwave squeezed states could be used to achieve high-fidelity quantum transduction in setups where the coupling is too weak to have $\mathcal{C} \sim 1$ (refs. [19–22]). Such protocols are uniquely suited to circuit QED, as Josephson-junction-based circuits can be used to realize large-gain, quantum-limited parametric amplifiers, which in turn act as sources of squeezed microwaves. Work has also demonstrated that the same kind of bosonic error-correcting codes that have been implemented in circuit QED for quantum information processing could also be exploited for noise-resilient quantum-state transfer[23].

Having established some of the basic concepts, we now discuss a variety of specific, circuit-QED hybrid-system architectures in more detail.

Circuit QED with mechanical oscillators

Systems of micromechanical oscillators have benefited spectacularly from their combination with circuit-QED techniques[10]. The union of these oscillators with superconducting resonant circuits creates a method for an otherwise classical system to inherit quantum behaviour. Indeed, macroscopic mechanical oscillators have quanta of motion whose energy is small compared with the thermal energy of the environment and respond linearly at the quantum scale. Consequently, their motion generally does not exhibit quantum features. Observing aspects of their motion that require a quantum description has been a long-standing goal of quantum science, motivated initially by the detection of gravitational waves, but also to probe whether there is a limit to the size or mass of an object that exhibits quantum behaviour[24,25].

Many aspects of this goal have now been achieved by electromechanical devices, in which motion of a mechanical oscillator with the resonance frequency ω_{m} alters the microwave resonance frequency ω_{c} of an LC-resonant circuit. In the most common approach, the mechanical oscillator's displacement $\hat{x}$ changes the separation between the two electrodes of the capacitor, thus parametrically coupling the electrical and mechanical systems at rate $g_0 = (\mathrm{d}\omega_{\mathrm{c}}/\mathrm{d}x)x_{\mathrm{zpm}} \approx \omega_{\mathrm{c}}(x_{\mathrm{zpm}}/2l)$, where x_{zpm} is the oscillator's zero-point motion and l is the static separation of the capacitor electrodes (Fig. 2a). The parameter $x_{\mathrm{zpm}}/2l$ is small, controlled by typical scales for micromechanical zero-point motion of $x_{\mathrm{zpm}} \sim 10^{-15}$ m and electrode separations that resist collapse from the Casimir force $l > 10^{-8}$ m. Consequently, g_0 is small compared with the circuit's quantum decoherence rate $\gamma_{\mathrm{c}}/2$ and comparable to the mechanical oscillator's decoherence rate ($n_{\mathrm{T}} = 1/2)\gamma_{\mathrm{m}}$, where γ_{c} and γ_{m} are the resonator and mechanical oscillator energy decay rates, respectively, and n_{T} is the thermal equilibrium number of phonons occupying the mechanical oscillator.
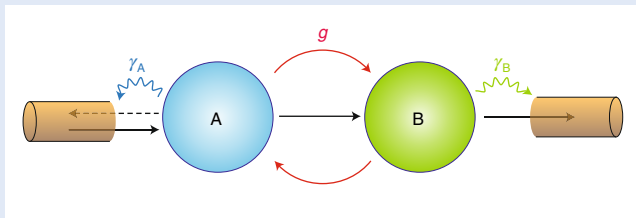
Box 2 | Cooperativity

In a hybrid quantum system, it is desirable to achieve a coupling g (which sets the frequency at which excitations are swapped back and forth between the subsystems) that is greater than some relevant measure of dissipation in each subsystem, such as decay or dephasing. If we characterize these processes by the rates γ_A and γ_B, then for some applications, one requires the stringent strong-coupling condition $g > \max(\gamma_A,\gamma_B)$. There are, however, a variety of important settings where one instead only requires the more forgiving condition $g \geq \sqrt{\gamma_A\gamma_B}$, that is, the coupling only needs to exceed the geometric mean of the dissipation rates. In these cases, the relevant figure of merit involves the cooperativity parameter $\mathcal{C}$ defined by:

$$\mathcal{C} = 4g^2/(\gamma_A\gamma_B) \quad (3)$$

When is the cooperativity relevant? It is the relevant figure of merit when, for example, the goal is to use one system to modify the dissipative environment of the other one. Each system experiences two kinds of dissipation: its intrinsic dissipation, and dissipation induced by the hybrid coupling. For example, B has its own intrinsic loss rate γ_B, and in addition, an induced loss rate mediated by A, which for small g is given by $4g^2/\gamma_A$. $\mathcal{C}$ is thus the ratio of these rates, and $\mathcal{C} \gg 1$ implies that the induced dissipation dominates. This can be used for cooling purposes, for example, when A and B have very different natural frequencies and thus thermal excitation numbers. The large cooperativity regime can also be exploited for reservoir engineering schemes[107], where the induced dissipation from system A stabilizes system B in a non-trivial state. For example, squeezed mechanical states have been prepared by coupling mechanical resonators to superconducting circuits[34].

The cooperativity is also relevant for hybrid state-transfer protocols involving itinerant, propagating states in a continuum that serve as input–output channels (for example, waveguides or transmission lines). $\mathcal{C} \gg 1$ implies that an initial quantum state of A will primarily decay via B. If the rate γ_B represents a coupling between system B and an input–output channel, then this decay corresponds to a state-transfer operation. The cooperativity is also relevant when the goal is itinerant quantum-state transfer. In such cases, both γ_A and γ_B represent couplings to effective input–output channels. The goal is to now have an excitation incident on system A (from its input–output channel) emerge, perfectly transmitted, in the input–output channel coupled to system B. Like in classical wave propagation, this perfect transmission requires coherently cancelling any reflections via an impedance matching. Here, this means that the two kinds of dissipation seen by each system must be equal, that is, one needs $\mathcal{C} = 1$.

Schematic showing perfect transmission from system A to B, something that is possible when the impedance matching condition $\mathcal{C} = 1$ is satisfied. The dashed arrow indicates no reflection from system A back to the input channel.

The prospect of observing quantum effects of motion in electromechanics would then appear to be remote. Not only is g_0 small but also the electrical and mechanical systems are far off resonance
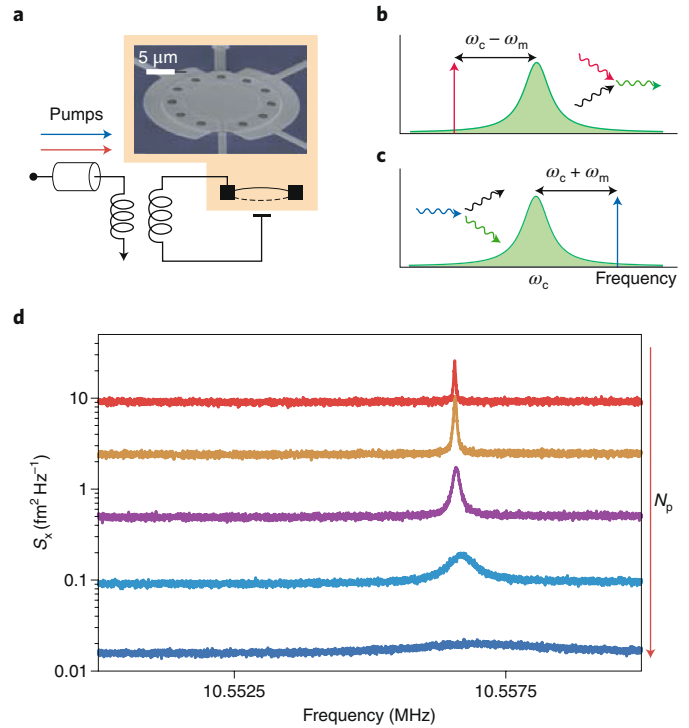
Fig. 2 | Electromechanics. a, A microwave LC resonant circuit with a mechanically compliant capacitor forms an electromechanical device. Signals and pump tones enter and exit the circuit through the adjacent transmission line. The image shows a capacitor formed from an aluminium drumhead suspended 50 nm above an aluminium disk. **b**, The frequency response of the circuit is shown with a microwave pump tone detuned from resonance by $\Delta = \omega_m$, where pump photons scatter to higher energy by extracting phonons from the mechanical oscillator. **c**, If the pump is applied above resonance, pump photons decompose into lower frequency photons and mechanical phonons. **d**, The spectral density S_x of the thermomechanical motion of a 10 MHz mechanical oscillator measured by pumping the circuit below resonance as in **b**. With increasing pump power, the measurement sensitivity improves and the mechanical oscillator is damped and cooled from an occupancy of 27 phonons (red) to less than 1 (blue). Panel **d** adapted with permission from ref. [31], Springer Nature Ltd.

with each other with $\omega_m \ll \omega_c$, further suppressing their coupling. A unique strategy avoided these problems by using a high-frequency 6 GHz dilatational mode of a film bulk acoustic-wave resonator with strong, resonant piezoelectric coupling to a tunable superconducting qubit[26]. This seminal result spawned a new field of quantum acoustics, now regarded as distinct from electromechanics. For the case of a low-frequency mechanical oscillator parametrically coupled to a high-frequency resonant circuit, both the small value of g_0 and the frequency mismatch are overcome by driving the circuit with a large amplitude pump tone, inducing N_p photons in the resonator and creating an effective linear interaction between electricity and motion[27]. In the presence of a strong pump, the electromechanical Hamiltonian takes the form

$$
\begin{aligned}
\hat{H}/\hbar = & \Delta\left(\hat{a}^\dagger\hat{a} + \tfrac{1}{2}\right) + \omega_m\left(\hat{b}^\dagger\hat{b} + \tfrac{1}{2}\right) \\
& + g_0\sqrt{N_p}\left(\hat{a}^\dagger + a\right)\left(\hat{b}^\dagger + \hat{b}\right)
\end{aligned}
\quad (4)
$$

where $\Delta = \omega_c - \omega_p$ is the detuning between the pump frequency ω_p and the cavity resonance. The pump amplitude now determines the

coupling rate between the two oscillators as $g = g_0\sqrt{N_p}$, which can be much greater than either the electrical or mechanical dissipative rates, even though g_0 is small. Furthermore, this coupling is resonant when $\Delta = \pm\omega_m$.

Although this simple Hamiltonian describes two linearly coupled harmonic oscillators, it is nevertheless capable of exhibiting a wide variety of behaviours. In the resolved sideband limit $\gamma_c \ll \omega_m$ and for the two cases $\Delta = \pm\omega_m$, the electromechanical system isolates two types of scattering[28]. When $\Delta = \omega_m$, a pump photon combines with a phonon to create a higher-energy photon at the circuit's resonance frequency, yielding a beamsplitter process that exchanges the state of the circuit and mechanical oscillator (Fig. 2b). In contrast, when $\Delta = -\omega_m$, a pump photon decays into a lower-energy photon at the circuit's resonance frequency and a phonon (Fig. 2c), resulting in a process that simultaneously amplifies the state of the circuit and mechanical oscillator. When $\Delta = 0$, both processes are equally likely, yielding a radiation pressure force on the mechanical oscillator with a quantum component from the shot-noise fluctuations in the number of pump photons. An even wider range of behaviours can be created by temporally varying $\Delta(t)$ and $N_p(t)$ or by applying more than one pump tone.

As for other coupled systems, the cooperativity $\mathcal{C} = 4g^2/\gamma_c\gamma_m$ is a crucial parameter, but because of the large equilibrium occupation of the low-frequency mechanical oscillator, quantum coherent coupling requires $\mathcal{C} > n_T$. Early work was able to achieve $\mathcal{C} > 1$ (ref. [28]), which allowed measurement of motion with precision needed to resolve the mechanical oscillator's zero-point motion[29]. By building the mechanical oscillators from suspended drumheads, the cooperativity increased dramatically[30], reaching the quantum enabled regime $\mathcal{C} > n_T$. In this regime, it is possible to cool the mechanical oscillator to its motional ground state[31] (Fig. 2d) and for the quantum radiation pressure force to dominate thermal forces[32]. With the capability to prepare mechanical oscillators in nearly pure quantum states, research then turned to creating states that exhibited entanglement between mechanical motion and microwave fields[33] or quantum squeezing of the mechanical oscillator[34]. Current work is focused on making more profoundly quantum 'non-Gaussian states' from three-element hybrid systems, consisting of mechanical oscillators, microwave resonators and superconducting qubits[35–37].

Finally, in a remarkable example of parallel evolution, advances in electromechanics were mirrored in the optical domain by the field of optomechanics[10]. The combination of optomechanics and electromechanics, in which a single mechanical oscillator alters both an optical and electrical resonance appears to be a promising approach to creating a quantum transducer between the microwave and optical domains, a key enabling technology for a future quantum network of quantum computers[38].

Quantum acoustics

Quantum acoustics (or quantum acoustodynamics) is a derivative from quantum electromechanics, making rapid progress in the past few years.

In quantum electromechanics discussed in the previous section, the target collective excitations are of the modes, such as flexural, torsional and breathing, in nanofabricated mechanical structures whose characteristic dimensions are comparable to the wavelength of the excitation. In contrast, in quantum acoustics, the focus is on acoustic modes typically with a much shorter wavelength than the device size. This allows us to easily access higher-frequency modes in the range of hundreds of megahertz to several gigahertz.

The acoustic waves propagate in a crystal with a sound velocity (of the order of 10^3 m s^{-1}) much smaller than that of electromagnetic waves. Thus, acoustic-wave devices are widely used as compact radio- and microwave-frequency components such as waveguides, resonators and filters. Both the acoustic modes propagating in the bulk and on the surface can be low loss, especially
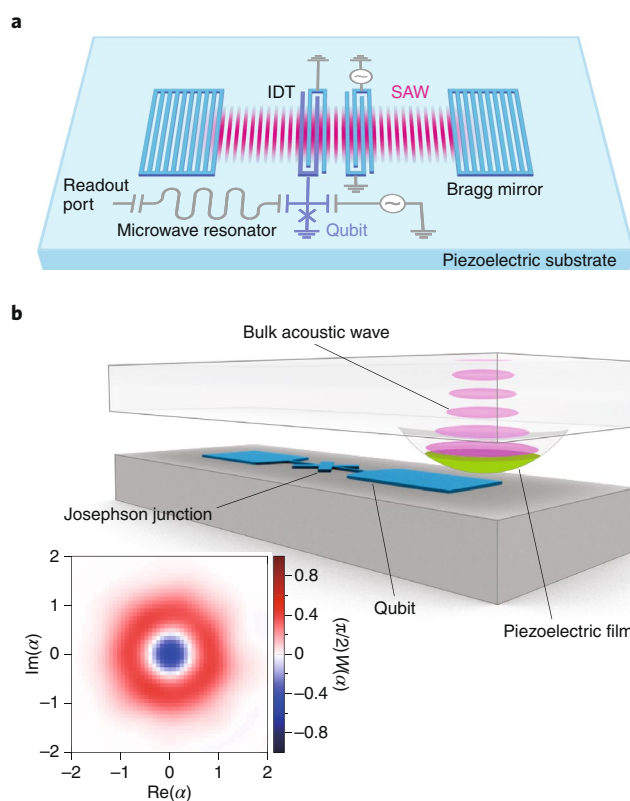

Fig. 3 | Quantum acoustics devices. a, Schematic of a SAW resonator coupled to a superconducting qubit through an IDT on the piezoelectric substrate. The SAW resonator mode is defined by the Bragg reflectors. The SAW excitation can also be driven coherently through an IDT. **b**, Illustration of a BAW resonator coupled to a superconducting qubit. The deformation associated with the bulk acoustic standing-wave mode induces an alternating electric field on a qubit electrode through the piezoelectricity of a film formed on the convex bottom surface of the upper substrate. The inset is a plot of the reconstructed Wigner function $W(\alpha)$ of the single-phonon Fock state observed in ref. [48]. Inset in panel **b** adapted with permission from ref. [48], Springer Nature Ltd.

at low temperatures, resulting in high-quality-factor resonators if properly confined[39,40].

For coupling with microwave-frequency electric circuits, the piezoelectric effect is used: an electric field across a piezoelectric material, such as quartz, AlN, LiNbO$_3$ and so on, induces deformation of the crystal lattice, and vice versa. The coupling can be much stronger than the typical radiation pressure interaction in electromechanical devices, providing unique opportunities in hybridization of the mechanical degrees of freedom with circuit-QED systems[26,41,42].

For example, in surface-acoustic-wave (SAW) resonators, acoustic waves propagating on the surface of a substrate (known as Rayleigh waves) — approximately within the depth corresponding to the wavelength — are confined horizontally by a pair of Bragg reflectors consisting of a comb-like array of electrodes fabricated on top of the substrate (Fig. 3a). The confined mode can be coupled with and driven electrically via interdigitated-transducer (IDT) electrodes, which are also like paired combs. Because of the vertical and horizontal confinement, the SAW resonators have small mode volumes, which enhances the vacuum fluctuation amplitudes of the modes and thus coupling with microwave circuits[43]. The resonant beamsplitter-type interaction between the acoustic and electric resonators gives rise to coherent exchange of a phonon and a photon[44–46].

Recently, coherent control of phononic states and generation of phonon Fock states were demonstrated both in SAW[47] and bulk-acoustic-wave (BAW)[26,48] resonators (Fig. 3b) resonantly coupled with a superconducting qubit through piezoelectricity. Quantum-state transfer and entanglement generation between two separated superconducting qubits were also demonstrated via a propagating SAW phonon released and captured by the qubits[49]. Phonon-number-resolved measurements in the strong dispersive coupling regime were also reported[50,51].

While the experimental techniques have been improving, the superconducting qubits fabricated on a piezoelectric substrate or coupled to an acoustic resonator tend to have limited coherence. Phononic-mode engineering to protect the qubits from spurious acoustic modes looks promising for future developments[50,51].

Coupling the phonons in an acoustic mode with photons in the optical domain is another challenge[16]. Photoelastic coupling could be a path for efficient transduction[52,53]. The architecture could be a direct electro-optical modulator type between a microwave resonator and an optical resonator or an indirect one with an acoustic resonator in between.

Quantum magnonics

The spin-dynamical counterpart to a phonon is a magnon. For simplicity, let us consider a lattice of a ferromagnetic insulator, in which localized spins are all aligned in the direction of an externally applied magnetic field. Because of the strong exchange interaction between neighbouring spins, the low-energy excitations are not individual spin flips, but long-wavelength collective precessional motions, that is, spin waves. The quantum of the harmonic-oscillator modes is a magnon.

Even though ferromagnetic resonance has been known for decades and the spin waves and magnons have attracted much interest in the context of spintronics, quantum manipulation and measurement of single magnons had not been in the scope of the previous studies until circuit QED brought the idea to initiate quantum magnonics.

The early attempts started with coupling magnons in a crystal of yttrium iron garnet (YIG), a ferrimagnetic insulator, to microwave photons in a coplanar resonator[54], followed by the observations of magnon–polariton modes in a three-dimensional cavity in the strong and ultrastrong coupling regimes[55–57]. In the latter experiments, the magnetic dipolar interaction strength of the 'macrospin' of a millimetre-scale sphere of YIG was enhanced up to the megahertz to gigahertz range by square-root of the total number (~10^{19}) of net electron spins as well as by the mode engineering of the three-dimensional microwave cavity.

Superconducting qubits are again exploited to bring anharmonicity to the coupled harmonic-oscillator system (Fig. 4a). Strong coupling between the qubit and the Kittel mode, that is, the spatially uniform ferromagnetic resonance mode, mediated by virtual photons in the detuned microwave cavity was achieved, and Rabi splitting of the qubit spectrum induced by a vacuum of magnons was observed[58] (Fig. 4b).

In the dispersive limit where the qubit and magnons are also detuned, a magnon-number-dependent qubit spectrum was reported[59] (Fig. 4c,d), similarly to the cases with microwave photons[60,61] and phonons[50,51]. Further progress towards single-shot detection of a magnon and applications to quantum sensing is expected[17]. An interesting proposal is to accelerate the search of axions, an unidentified candidate for dark matter, using magnons in ferromagnetic crystals[62,63].

The limited lifetime of magnons is currently a roadblock for drastic improvement of the quality factors in the quantum magnonics setup. Experiments indicate the presence of a bath of two-level systems, broadening the magnon linewidth to the range of 1 MHz at low temperatures[55,64,65]. Little is known about the ultimate magnon
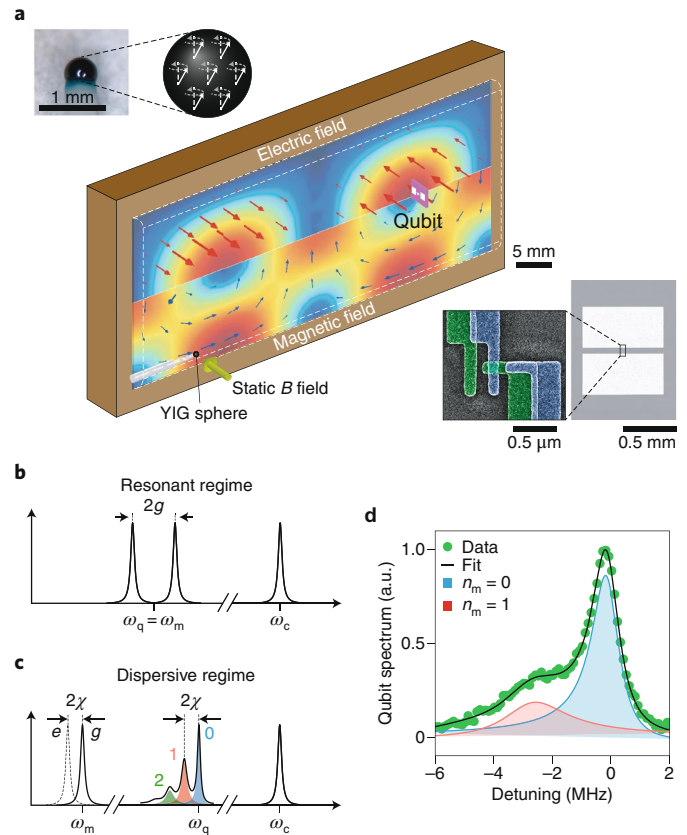

Fig. 4 | Quantum magnonics. a, Schematic of a setup for qubit–magnon coupling[58]. A ferromagnetic sphere of YIG is placed near the magnetic antinode of the microwave cavity mode (depicted in the lower half), while a superconducting transmon qubit is placed at the electric antinode (upper half). The sphere is under a localized static magnetic field $B \sim 0.3$ T to support the ferromagnetic resonance at ~10 GHz. The insets show the photographs of the sphere and the qubit. The Kittel mode in the sphere is also illustrated. **b**, Excitation spectrum in the resonant regime. The qubit (at the frequency ω_q) and magnon (ω_m) excitations, off-resonant from the cavity at ω_c, hybridize and show level-anticrossing by $2g$. **c**, Excitation spectrum in the strong dispersive regime. The qubit spectrum shows magnon-number-dependent splitting by the dispersive shift 2χ. The magnon spectrum is also split depending on the qubit state. **d**, Observed magnon-number-resolving qubit spectrum. From the fit, we can determine the occupation probability of the magnon-number (n_m) state in the Kittel mode. Panel **a** adapted with permission from ref.[58], AAAS.

lifetime in the low-temperature limit. Not many materials other than YIG are known for narrow-linewidth ferromagnetic (or anti-ferromagnetic) resonance, either, so inputs from material science would be helpful. Indeed, it would be interesting to see the physics of novel materials meet quantum magnonics and circuit QED. Quantum magnonics is an ultimate form of magnonics and spintronics, where excitations of a magnon can be a carrier of quantum information. Coherent interaction with light has also been investigated as optomagnonics and cavity optomagnonics[17].

Sensing and interfacing impurity spins with circuit QED

Circuit QED can also be fruitfully hybridized with dilute ensembles of electron spins that, contrary to spins in ferromagnetic materials, have negligible exchange interaction. Those are obtained for instance by doping a non-magnetic host crystal with paramagnetic impurities at the ppb–ppm level. At such low doping concentration,

the dipole–dipole interaction is also quite weak and spins can be considered as behaving independently. A typical spin-circuit-QED hybrid device is shown in Fig. 5a. Spins are coupled magnetically to the B_1 magnetic field generated by the inductive element of a superconducting microwave microresonator. They are also biased by a static B_0 field, applied in general parallel to the sample surface to minimize field-induced resonator losses, which shifts their frequency by the Zeeman effect and places them in resonance with the resonator. Many different spin systems can be used: nitrogen-vacancy centres in diamond, donors in silicon, rare-earth-ion-doped crystals and so on. Some of these systems (nitrogen vacancies, bismuth donors in silicon) have a zero-field splitting and thus need only a very low B_0 field (a few mT) to be placed in resonance with a superconducting microresonator whose frequency typically lies in the 3–10 GHz range, while others (phosphorus donors in silicon, some rare-earth-ion-doped crystals and so on) require fields in the 200 mT range, which can be conveniently applied if the resonator is made from Nb or NbTiN.

For typical microresonator geometries, the single spin-resonator coupling strength reaches $g/2\pi \sim$ 10 Hz–1 kHz. While this coupling is orders of magnitude lower than for transmon–resonator systems, it is still much larger than in usual magnetic resonance experimental setups, such that quantum fluctuations of the microwave field now play a major role, effectively bringing magnetic resonance spectroscopy into a novel quantum regime. The interest for quantum technologies of spin hybrid devices stems from the long coherence times obtained when the host crystal is magnetically silent (up to seconds for electron spins and hours for nuclear spins), as well as from their coherent coupling to other degrees of freedom (optical transitions, nuclear spins and so on). On this common ground, three research directions have emerged over the years.

First, circuit QED can be used to push electron paramagnetic resonance spectroscopy to ultimate limits in terms of spin detection sensitivity. Circuit QED helps in increasing the spin signal by providing large spin–resonator coupling and a high resonator quality factor, and also in reducing the noise by employing Josephson parametric amplifiers that provide ideal first-stage amplification for spin signals generated during Hahn echo pulse sequences (Fig. 5b). Several experiments reported spin detection sensitivity in the 10^2–10^4 spin $\sqrt{\mathrm{Hz}^{-1}}$ range[66–70], representing an improvement over the state of the art by several orders of magnitude. In these experiments, quantum microwave fluctuations not only impose a limit to the signal-to-noise ratio but also impact spin dynamics. Indeed, because of the large coupling constant and resonator quality factor, radiative relaxation may become the dominant channel for spins that are at resonance with the resonator if other intrinsic relaxation mechanisms (such as spin–phonon interactions) are weaker. This Purcell regime was reached for donors in silicon coupled to superconducting microresonators at millikelvin temperatures, where the spin relaxation time T_1 was reduced from 10^3 s to 1 s at resonance (Fig. 5c)[66]. In dense samples, radiation can occur collectively, by superradiant microwave emission[71]. Shortening T_1 also enables to repeat faster the measurements and therefore to improve on sensitivity. An ultimate sensitivity of 0.1 spin $\sqrt{\mathrm{Hz}^{-1}}$ is predicted to be possible[72], which would enable single spin detection, a challenging task that remains to be demonstrated. Circuit QED can also be used at another level, to generate non-classical microwave states with subshot-noise fluctuations on the signal quadrature, which leads to even higher spin detection sensitivity, as demonstrated recently with squeezed states[73].

Another natural idea is to use the electronic spin ensemble as a quantum memory, able to store quantum information at microwave frequency over timescales of the order of a second, or even hours if the state can be transferred to nuclear spins[14,74]. A key aspect is that an ensemble of N spins offers N nearly independent degrees of freedom where quantum information can be stored. As a result,
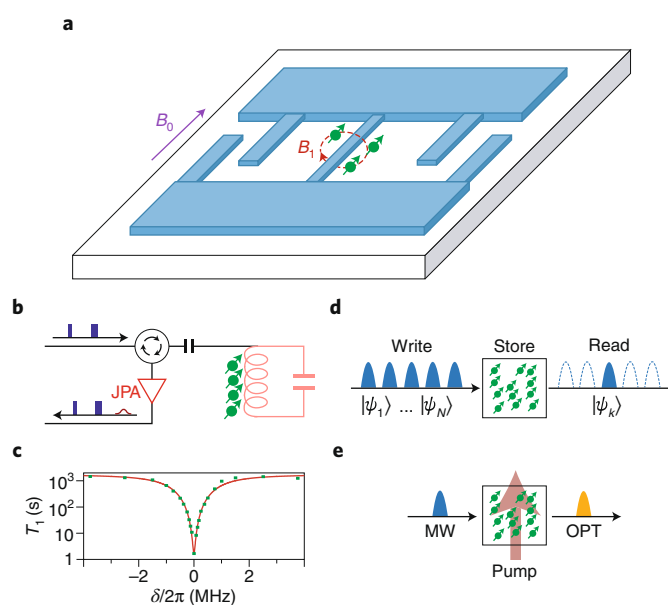

Fig. 5 | Quantum magnetic resonance. a, Schematic of a typical hybrid circuit-QED paramagnetic ensemble device. A superconducting resonator couples to a spin ensemble (green dots with arrows) via the a.c. magnetic field B_1 generated by the inductance. They are tuned at resonance by a d.c. magnetic field B_0 applied parallel to the substrate. **b**, Magnetic resonance with quantum microwaves. Ultrasensitive spin detection is achieved by applying Hahn echo sequences and amplifying the spin signal with a Josephson parametric amplifier (JPA). **c**, Cavity-controlled spin relaxation. The spin relaxation time T_1 is shown as a function of the spin-resonator detuning δ. Green squares are data and the red line is a fit to the Purcell relaxation rate plus a constant non-radiative decay[66]. **d**, Quantum memory. Trains of microwave pulses carrying quantum states ψ_i (i=1, …, N) are absorbed by the spin ensemble, stored and selectively retrieved on-demand. **e**, Coherent microwave (MW)–optical (OPT) conversion. An optical pump enables up-conversion of a microwave photon at optical frequency.

a single doped crystal interfaced by a single resonator may be used to store hundreds of single-microwave photon excitations originating from a superconducting quantum processor, and retrieve them on-demand for further processing (Fig. 5d). Experimentally, several building blocks of quantum memory proposals[75,76] have been demonstrated. Efficient absorption of an incoming microwave photon requires the ensemble cooperativity to be at least 1, which has been reached in several systems[77–80]. Interfacing with a superconducting qubit was also demonstrated[81,82]. Retrieving the absorbed excitation efficiently and noiselessly is, however, much more difficult. Protocols based on sequences of refocusing pulses were proposed, and steps towards their implementation were taken[83]; however, a fully operational spin-based quantum memory remains to be demonstrated.

Spin systems that have an optical transition are also attractive for microwave-to-optical coherent state conversion (Fig. 5e). Here, the spin ensemble provides the nonlinear medium that enables the mixing between microwave and optical fields under appropriate pumping conditions; resonators at both microwave and optical frequencies are required for enhancing the matter–field interaction; noiseless conversion is reached when the product of the microwave and optical cooperativities reaches 1 (ref. [84]). Rare-earth-ion-doped crystals seem particularly attractive for this purpose. A first experiment demonstrated spin-based magneto-optical conversion[85], although with an efficiency far from unity.

Coupling to quantum dots or single spins

As described in the previous section, there have been tremendous technical improvements in coupling large ensembles of spins to superconducting cavities in the circuit-QED architecture. The ultimate limit of circuit QED with spins would consist of an experiment in which a single spin is coherently coupled to a single photon. However, achieving single spin–photon strong coupling is challenging, as the coupling rate between the magnetic moment of a single spin and a single photon is of the order of 10 Hz (ref. [78]). Recently three separate experiments demonstrated strong coupling of spin states in quantum dots to microwave-frequency photons[86–88]. Instead of using direct magnetic coupling to the spin, these experiments hybridize the charge and spin degrees of freedom, to achieve spin–photon coupling rates $g_s/2\pi$ exceeding 10 MHz (ref. [89]).

Semiconductor quantum dots are lithographically defined structures (see Fig. 6 for an example) that can be used to isolate single charges and spins. Many experiments in mesoscopic physics are based on semiconductor double quantum dots (DQDs) and triple quantum dots (TQDs)[90,91]. DQD structures create a double-well confinement potential small enough to trap a single electron, with a gate-voltage-tunable interdot barrier height and energy-level detuning. Electric dipole coupling between this electron and a microwave-frequency photon can be achieved by embedding the DQD in a superconducting cavity[92–94]. Owing to the lithographic scale of a DQD, typically 200–500 nm across, the charge dipole moment can be much larger than a single atom, enabling the strong-coupling regime to be achieved with a charge–photon coupling rate $g_c/2\pi \geq$ 6.7 MHz (ref. [95]) A strong charge–photon coupling with an impressive $g_c/2\pi = 119$ MHz was demonstrated through the use of a high-impedance superconducting resonator[96].

Strong coupling to spin has been demonstrated in both DQD and TQD systems[86–89]. In DQDs, spin–electric coupling is generated using a combination of electric dipole coupling and spin–orbit interactions[89]. Spin–orbit interactions can be engineered by fabricating a micromagnet on top of the DQD[97]. The stray field of the micromagnet generates an extremely large magnetic field gradient of the order of 1 T μm⁻¹. A DQD spin in the magnetic field gradient will experience a spatially dependent magnetic field, the magnitude and direction of which depend on the position of the electron in the DQD[86]. By tuning the external magnetic field, the Zeeman splitting of the single electron spin can be brought into resonance with the cavity photon. In this configuration, the spin and photon coherently hybridize, leading to vacuum Rabi splitting in the cavity transmission spectrum[86,87]. These experiments showed that the spin–photon coupling rate $g_s/2\pi$ is a strong function of the DQD energy-level detuning, potentially allowing single spins to be coupled to a collective cavity mode 'on demand' for the implementation of long-range spin–spin quantum gates[98].

Recently, coherent spin–photon coupling using a TQD defined in a GaAs/AlGaAs heterostructure was demonstrated[88]. A TQD consists of three series of tunnel-coupled quantum dots. When loaded with three electrons, exchange interactions between the spins in adjacent quantum dots lead to a resonant exchange qubit, 'RX qubit', whose energy splitting can be tuned into resonance with the cavity photon. In contrast with the DQD approach, spin–photon coupling can be achieved with an RX qubit without the use of a micromagnet, and perhaps may be more readily scaled up into larger system sizes. In these experiments, vacuum Rabi splitting was observed, with a spin–photon coupling rate $g_s/2\pi = 31.4$ MHz exceeding both the qubit dephasing rate and cavity loss rate.

In addition to potentially enabling long-range cavity-mediated gates between spatially separated electron spins, spin–photon coupling is a powerful resource for quantum measurement. When a qubit is coupled to a cavity, the energy of a photon in a cavity is dependent on the state of the qubit. The so-called dispersive shift
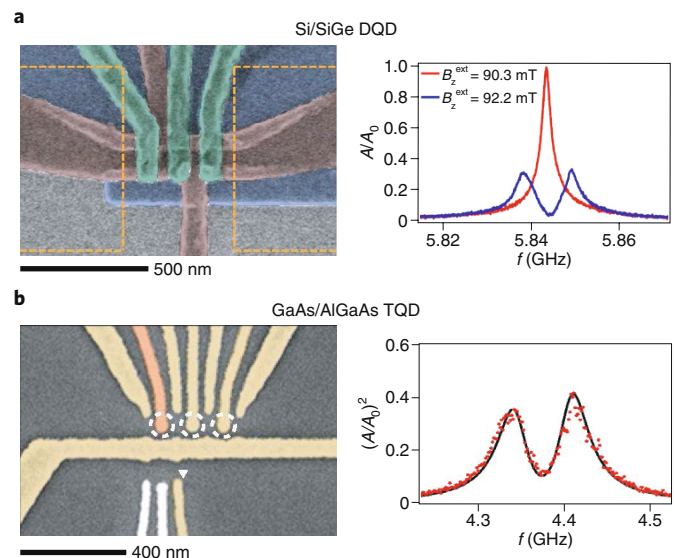

a   Si/SiGe DQD

b   GaAs/AlGaAs TQD

Fig. 6 | Strong spin–photon coupling. a, Left: scanning electron microscopy image of a Si/SiGe DQD. The DQD is used to isolate a single electron. The magnetic field gradient generated by a Co micromagnet (orange dashed lines) allows for spin–electric coupling. Right: vacuum Rabi splitting is observed when the Zeeman splitting of the single electron is tuned into resonance with the cavity photon. A/A_0 is the normalized cavity transmission in the spectroscopy, f is the frequency, and B_z^{ext} is the in-plane magnetic field applied to the device. **b**, Left: scanning electron microscopy image of a GaAs/AlGaAs TQD that is used to isolate three electrons, with one electron per dot. Right: vacuum Rabi splitting associated with tuning the resonant exchange spin qubit transition energy into resonance with the microwave cavity. Figure adapted with permission from: **a**, ref. [86], Springer Nature Ltd; **b**, ref. [88], Springer Nature Ltd.

has been used in the field of superconducting qubits for high fidelity[99] and multiplexed qubit readout[100]. Similarly, coherent spin–photon coupling enables dispersive readout of a single electron spin state, as recently demonstrated in ref. [86]. Another readout approach is based on singlet-triplet spin blockade, where tunnelling between the left and right sites of a DQD is suppressed in the two-electron regime when the electrons are in a spin triplet state[91]. Spin blockade was used to read out a cavity-coupled InAs nanowire spin–orbit qubit[93]. A recent experiment utilized a Si/SiGe DQD to demonstrate 98% high fidelity singlet-triplet readout in 6 μs (ref. [101]).

While 2018 was the year of strong spin–photon coupling[86–88], much work remains to convert these scientific achievements into a technology that will enable high-fidelity quantum gates between spatially separated spins. In these early demonstrations, the spin–photon coupling rates exceeded the cavity loss rates and spin-qubit dephasing rates by just a factor of two or three. Improvements in the spin–photon cooperativity can be achieved by using high-impedance superconducting resonators to boost $g_s/2\pi$, reducing cavity decay rates $\kappa/2\pi$ through improvements in cavity designs, and reducing spin dephasing rates $\gamma_s/2\pi$ through the use of isotopically enriched ²⁸Si. A recent demonstration of resonant spin–spin coupling through a microwave cavity provides encouragement for the long-term prospects of this quantum device technology[102].

In addition to gate-defined semiconductor quantum dots, several other hybrid quantum systems using single electrons and spins are being explored in combination with circuit QED. An interesting approach is to couple electrons confined to the surface of liquid helium to superconducting resonators[103,104,105].

Outlook

Circuit QED has proven its versatility and powerfulness as a tool for quantum control and measurement of other quantum systems in the microwave domain. With the improved and still improving coherence times ($\gtrsim$100 μs), gate and readout fidelities ($\gtrsim$99%), and integrated numbers ($\gtrsim$50) of superconducting qubits, as well as with the sophisticated circuit-QED techniques, we expect more advanced control of the target systems in future. There will be numerous applications in quantum transducing and sensing of faint signals at the single-quantum level with a quantum-limited transduction/measurement chain in the microwave domain. Synergy with condensed-matter physics in this aspect could be an exciting direction, for example, in the detection and manipulation of unidentified elementary excitations.

Furthermore, hybrid systems tremendously expand the potential of superconducting quantum circuits. An interface to optical quantum networks is something superconducting circuits cannot implement by themselves and definitely requires the assistance of other physical systems. Similarly, a long-distance quantum bus and long-lifetime quantum memory realized in hybrid systems may be useful in an architecture for superconducting quantum computers.

References

1. Nakamura, Y., Pashkin, Y. A. & Tsai, J. S. Coherent control of macroscopic quantum states in a single-Cooper-pair box. *Nature* **398**, 786–788 (1999).
2. Martinis, J. M., Devoret, M. H. & Clarke, J. Quantum Josephson junctions and the dawn of artificial atoms. *Nat. Phys.* https://doi.org/10.1038/s41567-020-0829-5 (2020).
3. Haroche, S. & Raimond, J.-M. *Exploring the Quantum* (Oxford Univ. Press, 2006).
4. Blais, A., Huang, R.-S., Wallraff, A., Girvin, S. M. & Schoelkopf, R. J. Cavity quantum electrodynamics for superconducting electrical circuits: an architecture for quantum computation. *Phys. Rev. A* **69**, 062320 (2004).
5. Wallraff, A. et al. Strong coupling of a single photon to a superconducting qubit using circuit quantum electrodynamics. *Nature* **431**, 162–167 (2004).
6. Haroche, S., Brune, M. & Raimond, J. M. From cavity to circuit quantum electrodynamics. *Nat. Phys.* https://doi.org/10.1038/s41567-020-0812-1 (2020).
7. Clerk, A. A., Girvin, S. M., Marquardt, F. & Schoelkopf, R. J. Introduction to quantum noise, measurement, and amplification. *Rev. Mod. Phys.* **82**, 1155–1208 (2010).
8. Poot, M. & van der Zant, H. S. Mechanical systems in the quantum regime. *Phys. Rep.* **511**, 273–335 (2012).
9. Xiang, Z.-L., Ashhab, S., You, J. Q. & Nori, F. Hybrid quantum circuits: superconducting circuits interacting with other quantum systems. *Rev. Mod. Phys.* **85**, 623–653 (2013).
10. Aspelmeyer, M., Kippenberg, T. J. & Marquardt, F. Cavity optomechanics. *Rev. Mod. Phys.* **86**, 1391–1452 (2014).
11. Cottet, A. et al. Cavity QED with hybrid nanocircuits: from atomic-like physics to condensed matter phenomena. *J. Phys. Condens. Matter* **29**, 433002 (2017).
12. Kurizki, G. et al. Quantum technologies with hybrid systems. *Proc. Natl Acad. Sci. USA* **112**, 3866–3873 (2015).
13. Degen, C. L., Reinhard, F. & Cappellaro, P. Quantum sensing. *Rev. Mod. Phys.* **89**, 035002 (2017).
14. Morton, J. J. L. & Bertet, P. Storing quantum information in spins and high-sensitivity ESR. *J. Magn. Reson.* **287**, 128–139 (2018).
15. Lambert, N. J., Rueda, A., Sedlmeir, F. & Schwefel, H. G. L. Coherent conversion between microwave and optical photons — an overview of physical implementations. Preprint at https://arxiv.org/abs/1906.10255 (2019).
16. Safavi-Naeini, A. H., Thourhout, D. V., Baets, R. & Laer, R. V. Controlling phonons and photons at the wavelength scale: integrated photonics meets integrated phononics. *Optica* **6**, 213–232 (2019).
17. Lachance-Quirion, D., Tabuchi, Y., Gloppe, A., Usami, K. & Nakamura, Y. Hybrid quantum systems based on magnonics. *Appl. Phys. Express* **12**, 070101 (2019).
18. Blais, A., Girvin, S. M. & Oliver, W. D. Quantum information processing and quantum optics with circuit quantum electrodynamics. *Nat. Phys.* https://doi.org/10.1038/s41567-020-0806-z (2020).
19. Filip, R. Quantum interface to a noisy system through a single kind of arbitrary Gaussian coupling with limited interaction strength. *Phys. Rev. A* **80**, 022304 (2009).
20. Zhang, M., Zou, C.-L. & Jiang, L. Quantum transduction with adaptive control. *Phys. Rev. Lett.* **120**, 020502 (2018).
21. Lau, H.-K. & Clerk, A. A. High-fidelity bosonic quantum state transfer using imperfect transducers and interference. *npj Quantum Inf.* **5**, 31 (2019).
22. Lau, H.-K. & Clerk, A. A. Ground state cooling and high-fidelity quantum transduction via parametrically-driven bad-cavity optomechanics. Preprint at https://arxiv.org/abs/1904.12984 (2019).
23. Xiang, Z.-L., Zhang, M., Jiang, L. & Rabl, P. Intracity quantum communication via thermal microwave networks. *Phys. Rev. X* **7**, 011035 (2017).
24. Caves, C. M., Thorne, K. S., Drever, R. W. P., Sandberg, V. D. & Zimmermann, M. On the measurement of a weak classical force coupled to a quantum-mechanical oscillator. I. Issues of principle. *Rev. Mod. Phys.* **52**, 341–392 (1980).
25. Marshall, W., Simon, C., Penrose, R. & Bouwmeester, D. Towards quantum superpositions of a mirror. *Phys. Rev. Lett.* **91**, 130401 (2003).
26. O'Connell, A. D. et al. Quantum ground state and single-phonon control of a mechanical resonator. *Nature* **464**, 697–703 (2010).
27. Regal, C. A., Teufel, J. D. & Lehnert, K. W. Measuring nanomechanical motion with a microwave cavity interferometer. *Nat. Phys.* **4**, 555–560 (2008).
28. Teufel, J. D., Harlow, J. W., Regal, C. A. & Lehnert, K. W. Dynamical backaction of microwave fields on a nanomechanical oscillator. *Phys. Rev. Lett.* **101**, 197203 (2008).
29. Teufel, J. D., Donner, T., Castellanos-Beltran, M. A., Harlow, J. W. & Lehnert, K. W. Nanomechanical motion measured with an imprecision below that at the standard quantum limit. *Nat. Nanotechnol.* **4**, 820–823 (2009). **This paper demonstrated efficient readout of a circuit QED system enabled by a Josephson parametric amplifier**.
30. Teufel, J. D. et al. Circuit cavity electromechanics in the strong-coupling regime. *Nature* **471**, 204–208 (2011).
31. Teufel, J. D. et al. Sideband cooling of micromechanical motion to the quantum ground state. *Nature* **475**, 359–363 (2011). **This paper showed that the radiation pressure force could cool a macroscopic mechanical oscillator to its motional ground state**.
32. Teufel, J., Lecocq, F. & Simmonds, R. Overwhelming thermomechanical motion with microwave radiation pressure shot noise. *Phys. Rev. Lett.* **116**, 013602 (2016).
33. Palomaki, T. A., Teufel, J. D., Simmonds, R. W. & Lehnert, K. W. Entangling mechanical motion with microwave fields. *Science* **342**, 710–713 (2013).
34. Wollman, E. E. et al. Quantum squeezing of motion in a mechanical resonator. *Science* **349**, 952–955 (2015).
35. Pirkkalainen, J. et al. Hybrid circuit cavity quantum electrodynamics with a micromechanical resonator. *Nature* **494**, 211–215 (2013).
36. Lecocq, F., Teufel, J. D., Aumentado, J. & Simmonds, R. W. Resolving the vacuum fluctuations of an optomechanical system using an artificial atom. *Nat. Phys.* **11**, 635–639 (2015).
37. Viennot, J. J., Ma, X. & Lehnert, K. W. Phonon-number-sensitive electromechanics. *Phys. Rev. Lett.* **121**, 183601 (2018).
38. Andrews, R. W. et al. Bidirectional and efficient conversion between microwave and optical light. *Nat. Phys.* **10**, 321–326 (2014).
39. Goryachev, M. et al. Extremely low-loss acoustic phonons in a quartz bulk acoustic wave resonator at millikelvin temperature. *Appl. Phys. Lett.* **100**, 243504 (2012).
40. Manenti, R. et al. Surface acoustic wave resonators in the quantum regime. *Phys. Rev. B* **93**, 041411 (2016).
41. Gustafsson, M. V. et al. Propagating phonons coupled to an artificial atom. *Science* **346**, 207–211 (2014). **This work pioneered the studies on the quantum regime of surface acoustic waves.**
42. Schuetz, M. J. A. Universal quantum transducers based on surface acoustic waves. *Phys. Rev. X* **5**, 031031 (2015).
43. Manenti, R. et al. Circuit quantum acoustodynamics with surface acoustic waves. *Nat. Commun.* **8**, 975 (2017).
44. Noguchi, A., Yamazaki, R., Tabuchi, Y. & Nakamura, Y. Qubit-assisted transduction for a detection of surface acoustic waves near the quantum limit. *Phys. Rev. Lett.* **119**, 180505 (2017).
45. Bolgar, A. N. et al. Quantum regime of a two-dimensional phonon cavity. *Phys. Rev. Lett.* **120**, 223603 (2018).
46. Moores, B. A., Sletten, L. R., Viennot, J. J. & Lehnert, K. W. Cavity quantum acoustic device in the multimode strong coupling regime. *Phys. Rev. Lett.* **120**, 227701 (2018).
47. Satzinger, K. J. et al. Quantum control of surface acoustic wave phonons. *Nature* **563**, 661–665 (2018).
48. Chu, Y. et al. Creation and control of multi-phonon Fock states in a bulk acoustic wave resonator. *Nature* **563**, 666–670 (2018).
49. Bienfait, A. et al. Phonon-mediated quantum state transfer and remote qubit entanglement. *Science* **364**, 368–371 (2019).

50. Arrangoiz-Arriola, P. et al. Resolving the energy levels of a nanomechanical oscillator. *Nature* **571**, 537–540 (2019). **This paper demonstrated phonon-number-resolving measurement of a nanomechanical oscillator interacting with a superconducting qubit in the strong dispersive regime**.

51. Sletten, L. R., Moores, B. A., Viennot, J. J. & Lehnert, K. W. Resolving phonon Fock states in a multimode cavity with a double-slit qubit. *Phys. Rev. X* **9**, 021056 (2019).

52. Rueda, A. et al. Efficient microwave to optical photon conversion: an electro-optical realization. *Optica* **3**, 597–604 (2016).

53. Fan, L. et al. Superconducting cavity electro-optics: a platform for coherent photon conversion between superconducting and photonic circuits. *Sci. Adv.* **17**, eaar4994 (2018).

54. Huebl, H. et al. High cooperativity in coupled microwave resonator ferromagnetic insulator hybrids. *Phys. Rev. Lett.* **111**, 127003 (2013).

55. Tabuchi, Y. et al. Hybridizing ferromagnetic magnons and microwave photons in the quantum limit. *Phys. Rev. Lett.* **113**, 083603 (2014).

56. Zhang, X., Zou, C.-L., Jiang, L. & Tang, H. X. Strongly coupled magnons and cavity microwave photons. *Phys. Rev. Lett.* **113**, 156401 (2014).

57. Goryachev, M. et al. High-cooperativity cavity QED with magnons at microwave frequencies. *Phys. Rev. Appl.* **2**, 054002 (2014).

58. Tabuchi, Y. et al. Coherent coupling between a ferromagnetic magnon and a superconducting qubit. *Science* **349**, 405–408 (2015). **This paper describes the demonstration of strong coupling between a magnon and a superconducting qubit**.

59. Lachance-Quirion, D. et al. Resolving quanta of collective spin excitations in a millimeter-sized ferromagnet. *Sci. Adv.* **3**, e1603150 (2017). **Demonstration of strong dispersive coupling between magnons and a qubit as well as magnon-number resolving measurement**.

60. Gambetta, J. et al. Qubit-photon interactions in a cavity: measurement-induced dephasing and number splitting. *Phys. Rev. A* **74**, 042318 (2006).

61. Schuster, D. I. et al. Resolving photon number states in a superconducting circuit. *Nature* **445**, 515–518 (2007).

62. Crescini, N. et al. Operation of a ferromagnetic axion haloscope at $m_a = 58 \mu ev$. *Eur. Phys. J. C.* **78**, 703 (2018).

63. Flower, G., Bourhill, J., Goryachev, M. & Tobar, M. E. Broadening frequency range of a ferromagnetic axion haloscope with strongly coupled cavity-magnon polaritons. *Phys. Dark Univ.* **25**, 100306 (2019).

64. Pfirrmann, M. et al. Magnons at low excitations: observation of incoherent coupling to a bath of two-level-systems. *Phys. Rev. Res.* **1**, 032023(R) (2019).

65. Kosen, S., van Loo, A. F., Bozhko, D. A., Mihalceanu, L. & Karenowska, A. D. Microwave magnon damping in YIG films at millikelvin temperatures. *APL Mater.* **7**, 101120 (2019).

66. Bienfait, A. et al. Controlling spin relaxation with a cavity. *Nature* **531**, 74–77 (2016). **Observation of the Purcell effect for spins**.

67. Sigillito, A. J. et al. Fast, low-power manipulation of spin ensembles in superconducting microresonators. *Appl. Phys. Lett.* **104**, 222407 (2014).

68. Eichler, C., Sigillito, A. J., Lyon, S. A. & Petta, J. R. Electron spin resonance at the level of 10^4 spins using low impedance superconducting resonators. *Phys. Rev. Lett.* **118**, 037701 (2017).

69. Probst, S. et al. Inductive-detection electron-spin resonance spectroscopy with 65 spins/ $\sqrt{\text{Hz}}$ sensitivity. *Appl. Phys. Lett.* **111**, 202604 (2017).

70. Budoyo, R. P. et al. Electron paramagnetic resonance spectroscopy of $Er^{3+}:Y_2SiO_5$ using a Josephson bifurcation amplifier: observation of hyperfine and quadrupole structures. *Phys. Rev. Mater.* **2**, 011403 (2018).

71. Angerer, A. et al. Superradiant emission from colour centres in diamond. *Nat. Phys.* **14**, 1168–1172 (2018).

72. Haikka, P., Kubo, Y., Bienfait, A., Bertet, P. & Moelmer, K. Proposal for detecting a single electron spin in a microwave resonator. *Phys. Rev. A* **95**, 022306 (2017).

73. Bienfait, A. et al. Magnetic resonance with squeezed microwaves. *Phys. Rev. X* **7**, 041011 (2017).

74. Grezes, C. et al. Towards a spin-ensemble quantum memory for superconducting qubits. *C. R. Phys.* **17**, 693–704 (2016). **Review of the experimental effort on quantum memories for microwave photons**.

75. Afzelius, M., Sangouard, N., Johansson, G., Staudt, M. U. & Wilson, C. M. Proposal for a coherent quantum memory for propagating microwave photons. *N. J. Phys.* **15**, 065008 (2013).

76. Julsgaard, B., Grezes, C., Bertet, P. & Molmer, K. Quantum memory for microwave photons in an inhomogeneously broadened spin ensemble. *Phys. Rev. Lett.* **110**, 250503 (2013).

77. Kubo, Y. et al. Strong coupling of a spin ensemble to a superconducting resonator. *Phys. Rev. Lett.* **105**, 140502 (2010). **This paper reports observation of strong coupling of a spin ensemble to a superconducting resonator**.

78. Schuster, D. I. et al. High-cooperativity coupling of electron-spin ensembles to superconducting cavities. *Phys. Rev. Lett.* **105**, 140501 (2010).

79. Amsüss, R. et al. Cavity QED with magnetically coupled collective spin states. *Phys. Rev. Lett.* **107**, 060502 (2011).

80. Probst, S. et al. Anisotropic rare-earth spin ensemble strongly coupled to a superconducting resonator. *Phys. Rev. Lett.* **110**, 157001 (2013).

81. Zhu, X. et al. Coherent coupling of a superconducting flux qubit to an electron spin ensemble in diamond. *Nature* **478**, 221–224 (2011).

82. Kubo, Y. et al. Hybrid quantum circuit with a superconducting qubit coupled to a spin ensemble. *Phys. Rev. Lett.* **107**, 220501 (2011).

83. Grezes, C. et al. Multimode storage and retrieval of microwave fields in a spin ensemble. *Phys. Rev. X* **4**, 021049 (2014).

84. Williamson, L. A., Chen, Y.-H. & Longdell, J. J. Magneto-optic modulator with unit quantum efficiency. *Phys. Rev. Lett.* **113**, 203601 (2014). **Proposal for microwave-optical photon conversion based on a spin ensemble**.

85. Fernandez-Gonzalvo, X., Chen, Y.-H., Yin, C., Rogge, S. & Longdell, J. J. Coherent frequency up-conversion of microwaves to the optical telecommunications band in an Er:YSO crystal. *Phys. Rev. A* **92**, 062313 (2015).

86. Mi, X. et al. A coherent spin–photon interface in silicon. *Nature* **555**, 599–603 (2018). **This article describes the demonstration of strong single spin–photon coupling and dispersive readout of the electron spin state**.

87. Samkharadze, N. et al. Strong spin–photon coupling in silicon. *Science* **359**, 1123–1127 (2018).

88. Landig, A. J. et al. Coherent spin–photon coupling using a resonant exchange qubit. *Nature* **560**, 179–184 (2018).

89. Cottet, A. & Kontos, T. Spin quantum bit with ferromagnetic contacts for circuit QED. *Phys. Rev. Lett.* **105**, 160502 (2010).

90. van der Wiel, W. G. et al. Electron transport through double quantum dots. *Rev. Mod. Phys.* **75**, 1–22 (2002).

91. Hanson, R., Kouwenhoven, L. P., Petta, J. R., Tarucha, S. & Vandersypen, L. M. K. Spins in few-electron quantum dots. *Rev. Mod. Phys.* **79**, 1217–1265 (2007). **The physics of spins in semiconductor quantum dots is thoroughly reviewed in this article**.

92. Frey, T. et al. Dipole coupling of a double quantum dot to a microwave resonator. *Phys. Rev. Lett.* **108**, 046807 (2012).

93. Petersson, K. D. et al. Circuit quantum electrodynamics with a spin qubit. *Nature* **490**, 380–383 (2012).

94. Viennot, J. J., Delbecq, M. R., Dartiailh, M. C., Cottet, a & Kontos, T. Out-of-equilibrium charge dynamics in a hybrid circuit quantum electrodynamics architecture. *Phys. Rev. B* **89**, 165404 (2014).

95. Mi, X., Cady, J. V., Zajac, D. M., Deelman, P. W. & Petta, J. R. Strong coupling of a single electron in silicon to a microwave photon. *Science* **355**, 156–158 (2017).

96. Stockklauser, A. et al. Strong coupling cavity QED with gate-defined double quantum dots enabled by a high impedance resonator. *Phys. Rev. X* **7**, 011030 (2017).

97. Tokura, Y., van der Wiel, W. G., Obata, T. & Tarucha, S. Coherent single electron spin control in a slanting Zeeman field. *Phys. Rev. Lett.* **96**, 047202 (2006). **The use of micromagnets for coherent spin control and spin–photon coupling can largely be attributed to this pioneering theoretical paper**.

98. Trif, M., Golovach, V. N. & Loss, D. Spin dynamics in InAs nanowire quantum dots coupled to a transmission line. *Phys. Rev. B* **77**, 045434 (2008).

99. Wallraff, A. et al. Approaching unit visibility for control of a superconducting qubit with dispersive readout. *Phys. Rev. Lett.* **95**, 060501 (2005).

100. Heinsoo, J. et al. Rapid high-fidelity multiplexed readout of superconducting qubits. *Phys. Rev. Appl.* **10**, 034040 (2018).

101. Zheng, G. et al. Rapid gate-based spin read-out in silicon using an on-chip resonator. *Nat. Nanotechnol.* **14**, 742–746 (2019).

102. Borjans, F., Croot, X., Mi, X., Gullans, M. J. & Petta, J. R. Resonant microwave mediated interactions between distant electron spins. *Nature* **577**, 195–198 (2019).

103. Lyon, S. A. Spin-based quantum computing using electrons on liquid helium. *Phys. Rev.* **74**, 052338 (2006).

104. Koolstra, G., Yang, G. & Schuster, D. I. Coupling a single electron on superfluid helium to a superconducting resonator. *Nat. Commun.* **10**, 5323 (2019).

105. Schuster, D. I., Fragner, A., Dykman, M. I., Lyon, S. A. & Schoelkopf, R. J. Proposal for manipulating and detecting spin and orbital states of trapped electrons on helium using cavity quantum electrodynamics. *Phys. Rev. Lett.* **105**, 040503 (2010).

106. Andrews, R. W., Reed, A. P., Cicak, K., Teufel, J. D. & Lehnert, K. W. Quantum-enabled temporal and spectral mode conversion of microwave signals. *Nat. Commun.* **6**, 10021 (2015).

107. Poyatos, J. F., Cirac, J. I. & Zoller, P. Quantum reservoir engineering with laser cooled trapped ions. *Phys. Rev. Lett.* **77**, 4728–4731 (1996).

Author contributions

All authors contributed to the writing, editing and revision of the manuscript.

Competing interests

J.R.P. and Princeton University have filed a non-provisional patent application related to spin–photon transduction (US patent application no. 16534431).

Additional information

Correspondence should be addressed to Y.N.

Peer review information *Nature Physics* thanks Peter Leek and Peter Rabl for their contribution to the peer review of this work.

Reprints and permissions information is available at www.nature.com/reprints.

Publisher's note Springer Nature remains neutral with regard to jurisdictional claims in published maps and institutional affiliations.